Advanced Steel Construction – Vol. 19 No. 2 (2023) 157–165
DOI: 10.18057/IJASC.2023.19.2.8

STUDY ON SEISMIC BEHAVIOR OF TRAPEZOIDAL CORRUGATED STEEL PLATE SHEAR WALL STRUCTURE WITH PEC COLUMN

Zhao-Sheng Huang [1, 2], Zhan-Zhong Yin [1, 3, *] and Bao-Yue Song [1]

[1] *School of Civil Engineering, Lanzhou University of Technology, Lanzhou 730050, China*
[2] *Gansu Institute of Architectural Design and Research, Lanzhou 730000, China*
[3] *Western Engineering Research Center of Disaster Mitigation in Civil Engineering of Ministry of Education, Lanzhou University of Technology, Lanzhou 730050, China*
** (Corresponding author: E-mail: yinzhanzhong@lut.cn)*

ABSTRACT

This paper has carried out experimental and numerical research on the hysteretic characteristics of a corrugated steel plate shear wall which has a partially encased composite (PEC) column (PEC-CSPSW). Two single layer PEC-CSPSW cycle tests were conducted. For the sake of simulating the experimental results, the writer made a numerical model and verified it. The capacity of energy dissipation and failure mode of the structure were studied. The results displayed the PEC-CSPSWs had excellent bearing capacity, ductility, and energy dissipation feature, and the bearing capacity declined gradully. The PEC composite column could heighten the frame column's stiffness, enhance the steel plate anchoring effect , and then give full play to its post-buckling strength. The effects of the thickness, wavelength, wave height of the corrugated steel plate, and the strength of concrete on the lateral force resistance were analyzed. The results indicated that, under the rational parameter design, the CSPSW proposed in this paper had a high bearing capacity and strong energy dissipation feature. Besides, it was an ideal lateral force resisting and energy dissipation member.

ARTICLE HISTORY

Received: 2 September 2022
Revised: 15 January 2023
Accepted: 20 January 2023

KEYWORDS

Partially encased composite column;
Corrugated steel plate shear wall;
Low-cycle reverse loading test;
Seismic performance;
Finite element method (FEM);
Parametric investigation

Copyright © 2023 by The Hong Kong Institute of Steel Construction. All rights reserved.

1. Introduction

As an effective component to resist lateral force, steel plate shear wall(SPSW) has been widely concerned and developed in the past few years. Non-stiffened steel plate walls resist horizontal loads through diagonal tension bands of steel plates, but thin SPSWs are prone to instability and thick SPSWs cost more. Corrugated steel plates, because of their special structure, have a very small compressive stiffness along the corrugation direction (wave propagation direction), and a much higher compressive stiffness perpendicular to the corrugation direction than steel plates with the same thickness. Meanwhile, thin corrugated steel plates have a larger buckling strength and out-of-plane stiffness. Therefore, introducing a corrugated steel plate into the SPSWs can make up for the shortcoming that the thin SPSWs is apt to lose stability and costs less than the thick SPSWs. A trapezoidal steel plate is used to form a double lateral force resisting structure with the surrounding frame to resist seismic force.When the corrugated ribs are arranged along the vertical direction, the higher cylinder stiffness along the corrugated ribs can effectively resist the vertical load caused by partial gravity. Therefore, the corrugated steel plate shear wall(CSPSW) can meet the current code requirements that the embedded plate will not buckle during construction and normal use. The research on resistance to the lateral force of the CSPSW structure has drew the interest of many scholars.

An experimental study on corrugated steel plates with 45 oblique folds was conducted by Berman and Bruneau [1]. The results of the test demonstrated that the folds in the steel plate could prominently enhance the stiffness and ductility of the members, and strengthen the structure energy dissipation capacity. Botross and Lan [2-3] both proposed the concept of a corrugated steel plate wall and carried out finite element method analysis and research, Their results showed that corrugated steel plate wall had great initial stiffness, brilliant hysteretic performance, and high energy dissipation capacity. Lu and Li [4] put forward a new type of buckling-restrained steel plate shear wall. They carried out loading tests which are monotonic and cyclic and focus on four groups of specimens with different aspect ratios, and completed the comparison test with ordinary SPSWs. Stajadinovic and Tipping [5] carried out hysteretic tests on 44 groups of light cold-formed corrugated steel plate walls, studied the seismic performance of light CSPSW, and proposed the recommended values of elementary parameters for the seismic design of light CSPSWs. LA Fülöp and I Hakola [6] proposed an analytical design method for light-gauge steel shear walls with thin sheet sheaths. Finite element simulations and experiments verified the effectiveness of this method. The comparison showed that it had good accuracy when evaluating strength, but the stiffness evaluation was not satisfactory.

Johnson et al. [7] studied the ultimate bearing capacity and shear elastic stiffness of corrugated steel web beams based on finite element analysis and experiment. Liu et al. [8]used the Galerkin method to derive the analytical formulas of the integral and interactive shear buckling stress of corrugated steel webs. A simplified formula of the shear buckling coefficient k_g of corrugated steel webs was given. Zhao et al. [9] showed through experiments that the corrugated steel plate shear wall structure had large initial stiffness, high bearing capacity, and minor out-of-plane deformation, which could enhance the pinching effect of the non-stiffened SPSW and made the hysteretic curve fuller. Dou et al. [10-11] studied the lateral bearing capacity and post-buckling performance of sinusoidal CSPSWs under unidirectional loads, and proposed a fitting formula to predict load-displacement curves.

Cao and Huang [12] discussed the hysteretic behavior of a double-layer single-span corrugated steel wall, and proposed its plate-frame interaction model under lateral load. In the above research, H-section steel columns were mostly used as the SPSWs's vertical edge members. However, under the additional influence of the steel plate tension field, the H-section steel columns were prone to premature local buckling, making the frame columns flexural and torsional unstable, and the effective anchorage of thin steel plate walls was lost, which was not conducive to the performance of SPSWs after buckling [13-15]. The partially encased composite (PEC) columns had a high bearing capacity, good ductility, fire resistance, seismic resistance, and convenient and economical manufacturing [16-20]. Therefore, some studies, introduced it into the non-reinforced SPSWs as a boundary element to provide reliable anchorage for the steel plate tension field expansion to solve the concave deformation and stability failure problems caused by the weak rigidity of the pure steel column [21-23]. Therefore, in this paper, the PEC column was applied in the CSPSWs by bolt connection, so that it became the edge member with a horizontal bearing capacity in the CSPSWs, provided strong anchoring force, and could bear high axial pressure, thus solving the concave deformation and stable damage of the pure steel column with weak rigidity and realizing the design philosophy of "strong frame and weak steel plate." The purpose was to explore the seismic performance of trapezoidal corrugated SPSWs with PEC columns. This paper made an experimental research on PEC-CSPSWs scale specimens. It analyzed the stiffness, energy dissipation performance, distribution and development of plastic deformation, and the structure failure mode. On the basis of verifying the finite element approach, the parameter research regarding to the height-thickness ratio of the steel plate, wavelength, and wave height of the corrugated plate, and the column concrete strength grade was carried out.

2. Experimental program

2.1. Specimen device and material characteristics

Two prefabricated PEC-CSPSWs specimens were used in this test, numbered PEC-CSPSW1 and PEC-CSPSW2 respectively. The PEC column

adopted double channel steel section, and the frame adopted H-shaped beam. The embedded trapezoidal corrugated plate was linked with the channel steel by friction type high-strength bolts, welded with the beam's lower flange, and the beam's web was connected with the column by bolts through the connecting plate welded on the flange of the column. In addition, φ 6 tensile steel bars were welded between channel steel flanges and concrete was poured to form specimens. At the test piece bottom, a 30mm thick steel plate was welded, which was connected to the reaction floor through the anchor rod. Through the material sample test, the steel material properties used in the sample were evaluated, as shown in Fig. 1. The sample design and specimen photos are shown in Fig. 2 and 3, respectively, and the geometric parameters of the corrugated plate can be detected from Fig. 4. The steel used in the test piece was Q235B, and the material test results are illustrated in Table 1. The concrete filled in the PEC column was C30, and the cubic compressive strength after 28 days was 31.5N/mm2. The Young's modulus of filled concrete was 3.2×104N/mm^2. Beam-column-infill plate connection adopted friction high-strength bolts with an ultimate strength of 1230MPa and a yield strength of 940MPa.

Fig. 1 Test of specimen material properties

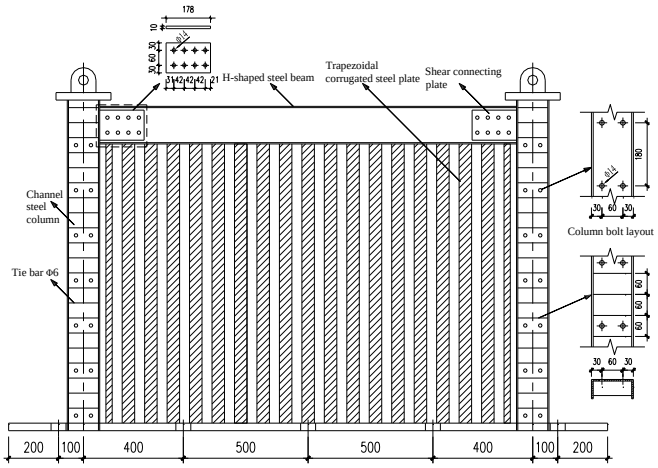

Fig. 2 Dimensions and details of specimens

Fig. 3 Pictures of PEC-CSPSW specimens

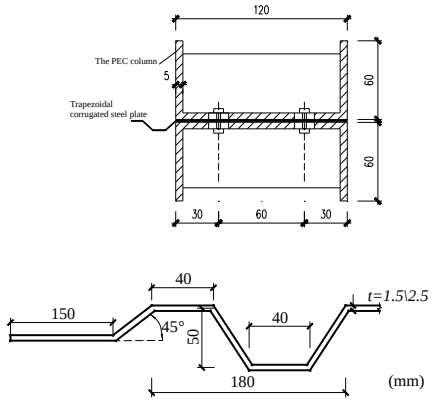

Fig. 4 Geometric parameters of vertical trapezoidal corrugated plate

Table 1
Material proprieties of steel

Item	f_y / *MPa*	f_u / *MPa*	*E* / *MPa*	δ / %
1	269.2	390.1	1.97	22.12
2	256.7	380.7	1.93	20.83
3	257.8	405.8	1.99	23.51
4	254.5	379.6	2.01	22.04
5	262.4	377.8	1.87	25.35
6	253.9	391.4	2.09	24.36
7	263.6	384.6	2.07	26.03
8	247.4	386.0	1.99	23.43
9	245.2	399.7	1.97	21.93
10	238.6	396.8	2.04	25.76
The average	254.9	389.2	1.99	23.53

f_y is yield stress; f_u is ultimate stress; E is the elastic modulus; δ is tensile elongation.

2.2. Loading protocol and instrument

The low-cycle repeated horizontal displacement loading method was adopted to test the mechanical performance of the specimen under earthquake action. Before the formal loading, pre-load was used to eliminate the pre-tightening force generated by the MTS loading end and loading beam end.

Constant amplitude cyclic loading with yield displacement Δ_y as multiple was adopted in the loading process. Each level was loaded for 3 times, first pushed and then pulled. When the sample is damaged or the load drops to 85% of the peak load, the test finished. Lateral supports with supports were arrayed on both sides of the intermediate part of the frame to prevent the specimen from buckling. [24].

The arrangement of measuring instruments is shown in Fig. 7. T-shaped resistance strain gauges were arranged on the main diagonal, and 1/3 diagonal of the embedded steel plate, the key parts of beams and columns, were also provided with a one-way resistance strain gage.A total of 104 strain collection points were laid out for each specimen, including 96 on steel and 8 on concrete. At the same time, a resistance displacement meter was arranged in the key parts of the plate to monitor the deformation of each position in the test.

2.3. Failure mode and damage procedure

The PEC-CSPSW1 specimen had no obvious phenomenon under the first two cyclic loads. When the load was pushed to 9mm(D=0.75%), the steel plate surface buckled slightly. At this time, there was no obvious phenomenon on the concrete surface, the deformation disappeared after unloading, and the plate was in the elastic stage. The buckling wave deformation became more obvious when the loading displacement was close to 15mm (D=1.25%). As the loading displacement increased, the buckling wavelength slowly increased, forming diagonal tensile bands from the upper left to the lower right, and the structure entered an elastic-plastic state. When the displacement was loaded to 21mm(D=1.75%), two oblique folds were formed in the center of the steel plate wall. Then, the bolt rod rubbed violently with the steel plate, producing a “squeaking” sound. When the loading displacement reached 33mm(D=2.75%), two large “X” shapes were formed by folding and crossing the front and back of the steel plates, and the steel plate at the center of the fold appeared convex corner, accompanied by the tearing of the steel plate. Most “X”-shaped tension bands had openings due to the tearing of steel plates at the center when loaded to 42mm(D=3.5%). Along with the reciprocating change of displacement, the degree of the opening increasingly grew, and the color of the steel around the opening became dark with burning marks. At this time, the yield area of steel plates increased slowly. The concrete surface in the PEC column was still intact when the load reached 45mm(D=3.75%), the yield range of the steel plate was not obviously increased, and the peak load in the load-displacement curve was not obviously decreased. The test stopped until the load reached 51mm(D=4.25%). Fig. 8 is the deformation diagram of the specimen.

Similar to PEC-CSPSW1, PEC-CSPSW2 was basically unchanged at the initial loading stage. When the displacement was loaded to 15mm (D=1.25%), the steel plate would buckle, and the deformation occured in the middle of the plate, which was about 50mm higher to the left than the buckling deformation position of specimen 1. After loading to 33mm(D=2.75%), the concrete surface of PEC column near the loading end has transverse cracks., and the area of steel plate folds increased. When loaded to 39mm(D=3.25%), the steel plate corner was torn, the steel plate yielded to a great extent, and the yield area increased slowly. As the load reached 42mm(D=3.5%),the steel plate tearing phenomenon became more obvious, the opening became larger, and the original cracks on the concrete surface became wider and longer. At this time, observing the load-displacement curve, the bearing capacity decreased little. With the load reaching 45 mm (D=3.75%), the corners of the “X”-shaped fold area basically showed openings, and the bearing capacity of the PEC column decreased greatly on account of different degrees of separation between flange and concrete, so the test was stopped. It is illustrated inFig. 9 the failure mode of specimen 2.

Under the horizontal load action, the two specimens achieved post-yield buckling, and both specimens were in the pure shear state before buckling, which fully developed plastic energy dissipation. After buckling, the tension band formed by buckling continued to uphold the load. Compared with the displacement requirements of the current code, it can be found that the edge frame of the structure kept elasticity under frequent earthquakes, and the steel plate consumed energy in buckling and shearing. Under rare earthquakes, the wallboard began to crack, but the structure had a certain loading capacity, and the loading capacity decreased slowly.

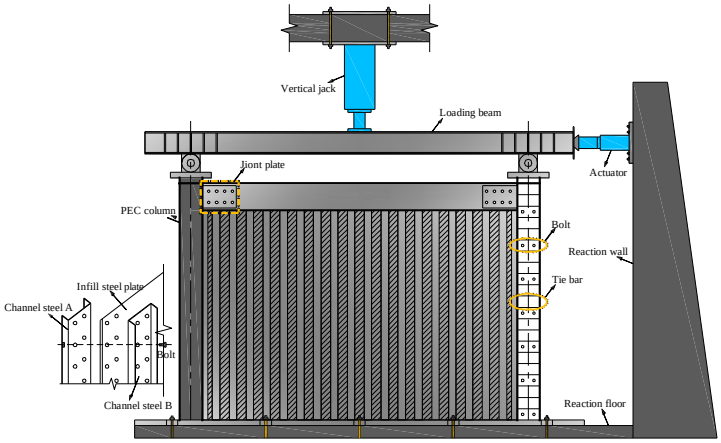

Fig. 5 Test setup

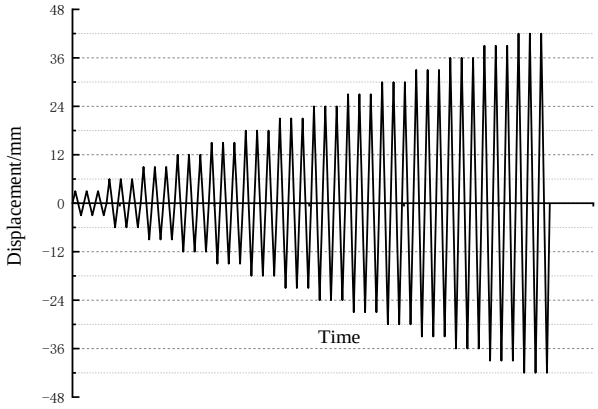

Fig. 6 Loading protocol

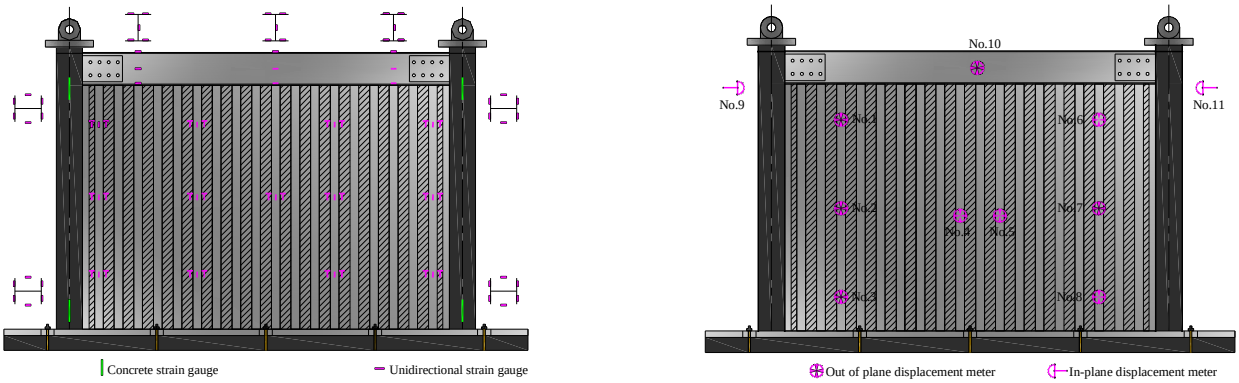

(a)Strain gauge layout

(b) Displacement gauge layout

Fig. 7 Layout of measuring instruments

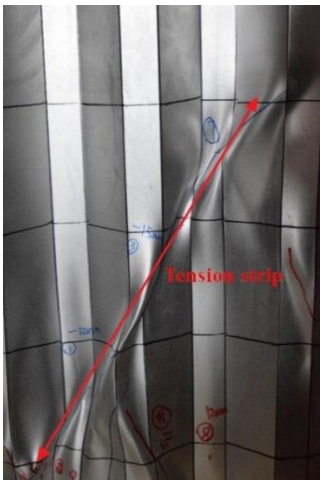

(a)Partial deformation when D=1.25%

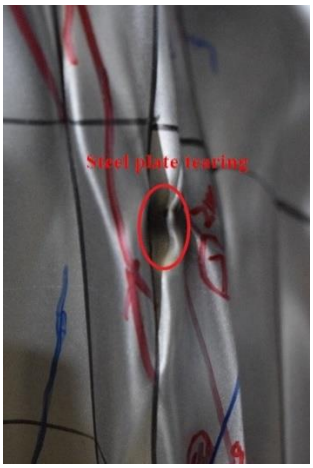

(b)Steel plate tear burn mark when D=3.5%

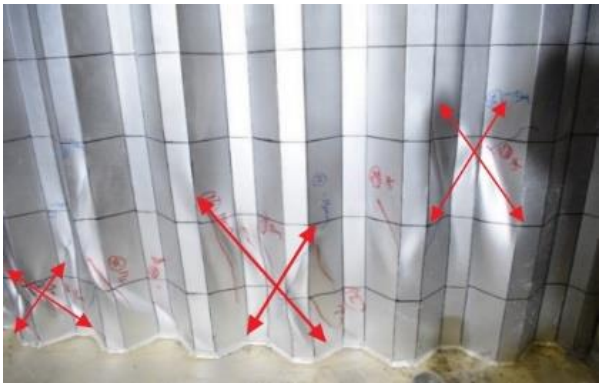

(c)Partial deformation when D=1.75%

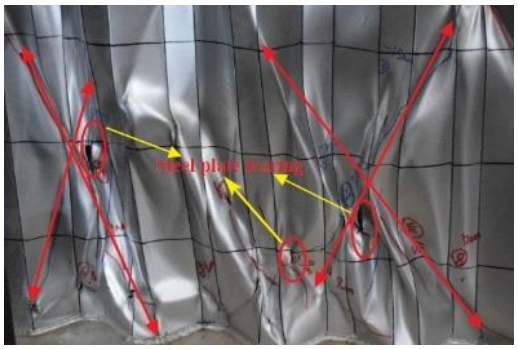

(d)The steel plate tears when D=3.5%

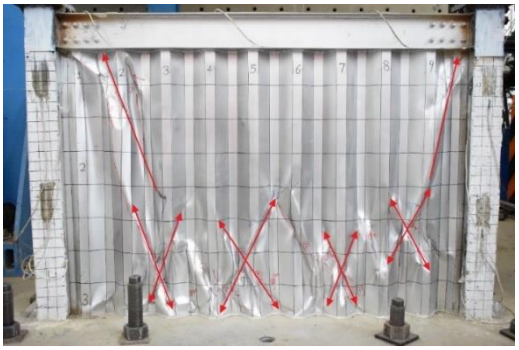

(e) Overall deformation when D=4.25%

Fig. 8 Failure mode of PEC-CSPSW1

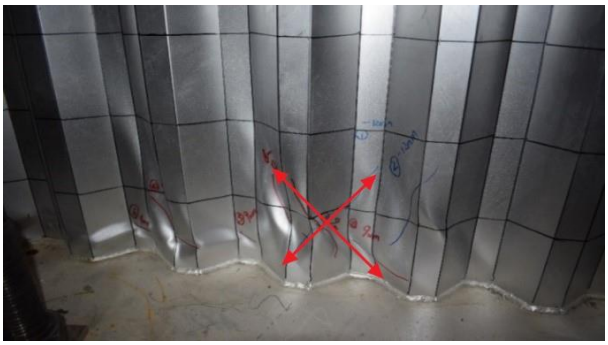

(a)Partial deformation when D=1.75%

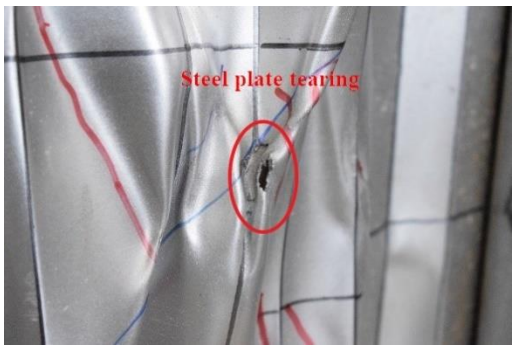

(b) The steel plate tears when D=3.25%

(c) The development of concrete cracks

Fig. 9 The failure mode of PEC-CSPSW2

2.4. Hysteretic behavior

The hysteretic curves of two specimens are diaplayed in Figure 10, both of which showed good working performance. The overall shape of the two specimens' hysteretic curves was cross-shaped, which was full and spindle-shaped at the initial loading stage. The shear resistance reached the maximum when the displacement was 10mm and 15mm, respectively, and then gradually began to decline, which is due to the stress state change from the overall shear resistance to the tension band shear resistance. As the displacement increased, the hysteretic loop area slowly increased, the shape gradually changed from spindle to bow, the

hysteretic curve reached a platform section, and the bearing capacity no longer decreased. As the plate began to tear, the pinch phenomenon became more and more obvious, and finally, it changed to a reverse S-shape. Specimens 1 had a smaller hysteretic area and lower yield capacity than specimens 2.

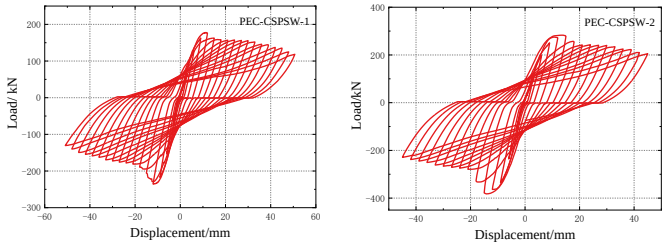

Fig. 10 Hysteretic curves of the specimen

2.5. Skeleton curves

The specimen's skeleton curve was symmetrical about the center of the coordinate origin. Furthermore, the value of the structure's initial stiffness was very large. The complete curve includes three stages: elasticity, strengthening, and plasticity. From the figure, we can find that on the elastic phase, the two specimens' skeleton curves rose linearly, and both of them had good initial stiffness. In the strengthening stage, it can be found that when reaching the yield load, the specimen's bearing capacity did not decrease immediately. This indicates that the specimens had preferable energy dissipation stability. When the specimen was on the plastic phase, the bearing capacity decreased, but the decreasing rate was relatively slow and still had a high bearing capacity.

Fig. 11 shows the comparison of skeleton curves. It shows that both specimens achieved post-buckling with relatively high initial bearing capacity. With the displacement increase, the skeleton curve showed a downward segment, but still had a fixed post-buckling bearing force. Among them, the performance of specimen 2 was more outstanding.

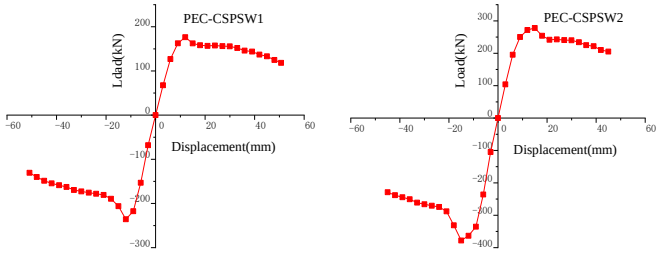

（a）PEC-CSPSW-1 （b）PEC-CSPSW-2

Fig. 11 Skeleton curves of the specimens

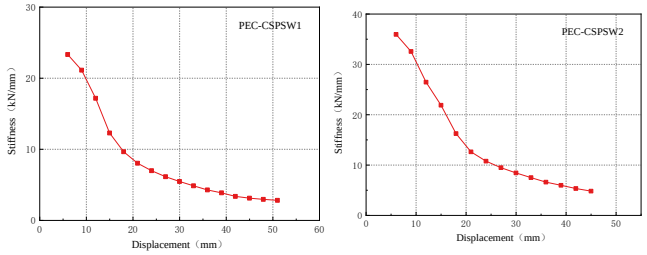

（a）PEC-CSPSW-1 （b）PEC-CSPSW-2

Fig. 12 Stiffness degradation curves of specimens

2.6. Stiffness degradation

Fig. 12 diaplays the specimens' stiffness degradation curve. It demonstrates that the stiffness degradation curves of PEC-CSPSW-1 and PEC- CSPSW-2 had the same general variation rule. As the displacement increased, the structure's global stiffness declined. The corrugated steel plates buckled with the loading displacement increase, the bearing capacity decreased greatly, and the stiffness degradation rate was high. On the middle and late phases of loading, the stiffness degradation rate slowed down, because, the surface of the corrugated steel plate has more tension bands, which could share the more lateral load, and the decline of bearing capacity was relatively stable.

2.7. Ductility and energy dissipation capacity

Table 2 lists the specimen's ductility coefficient. It demonstrates that the displacement ductility coefficient of PEC-CSPSW2 was higher than PEC-CSPSW1. The maximum peak load of PEC-CSPSW2 was 363.21kN when the displacement load was 15mm, which was 54.1% higher than that of PEC-CSPSW1. Results showed that the smaller the height-thickness ratio of the embedded trapezoidal corrugated steel plate, the greater the stiffness of the structure, meanwhile the bearing capacity of the structure is higher.

Table 2
Ductility of specimens

Item	$K_i(kN/mm)$	$P_y(kN)$	$P_m(kN)$	$P_u(kN)$	μ
PEC-CSPSW1	21.14	126.82	235.70	149.37	4.45
PEC-CSPSW2	32.57	195.44	363.21	228.97	5.56

K_i represents the initial stiffness; P_y represents yielding load; P_m represents peak load; P_u represents ultimate load; μ represents ductility coefficient.

The enveloping area of the hysteresis loop had the same energy dimension, which could reflect the energy consumption of the hysteresis loop. With larger area, more energy will be consumed. The energy consumption coefficient E was calculated as follows.

$$E = \frac{S_{ABC} + S_{CDA}}{S_{OBE} + S_{ODF}} \tag{1}$$

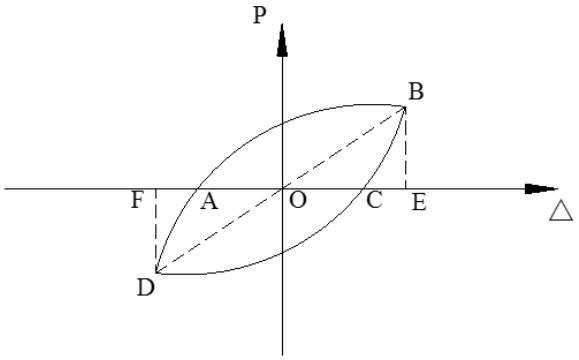

Fig. 13 The schematic diagram of the energy consumption coefficient

Table 3
The energy consumption coefficient

Item	PEC-CSPSW1	PEC-CSPSW2
E	2.25	2.76

Table 3 shows that, the two specimens' energy dissipation coefficient were greater than 2.0, and both of them had excellent energy dissipation ability. As the growth of the thickness of the corrugated steel plate, the overall stiffness of the structure accumulated, and the energy dissipation feature of the corrugated steel plate increased.

3. Finite element analysis of specimen

3.1. FEA model

FE software ABAQUS was adopted to simulate the model which adopted the same geometric size as the two specimens in the test. Columns, beams and wall plates were all made of linear reduced shell element (S4R) considering large deformation and small strain, and the core concrete was made of eight-node linear reduced hexahedral element (C3D8R).The contact relationship between concrete and channel steel was considered in the tangential and normal directions. Tangential friction was adopted, and the Coulomb friction coefficient of 0.3 was specified to reflect the bond and slip between channel steel and concrete. The normal direction adopted "hard contact". In addition, the out-of-plane freedom of the frame beam's flange was limited to simulate the out-of-plane constraint effect in the test. The model chart is displayed in Fig.14 and Fig.15.

The command "imperfections" was used in ABAQUS to include 3/1000b geometric defects extracted from buckling analysis in the model. To keep the

interface in contact, the initial defect values of the concrete and steel plate were the same. The elastic-linear hardening model and follow-up hardening rule were selected for steel, the hardening modulus , and Poisson's ratio in the elastic stage was 0.3. The constitutive relation of concrete was selected from the stress-strain expression of concrete proposed in reference [25], which considered the constraint effect of section steel. Table 4 shows the parameters of the concrete's plastic damage model.

Table 4
Plastic coefficients of concrete

$\alpha(°)$	e	σ_{b0}/σ_{c0}	K_c	γ
30°	0.1	1.16	2/3	0.0001

Therein, $\alpha(°)$ represents the dilation angle; e represents the eccentricity; σ_{b0} represents the initial equiaxial compressive yield stress; σ_{c0} represents the initial uniaxial compressive yield stress; K_c represents the second stress invariant ratio, and γ is the viscosity parameter.

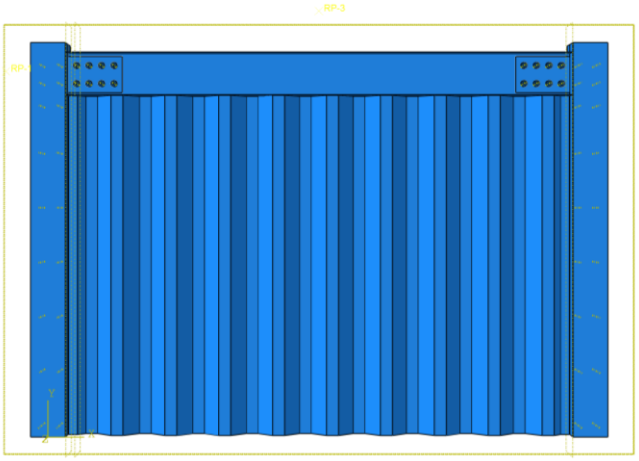

Fig. 14 The finite element model

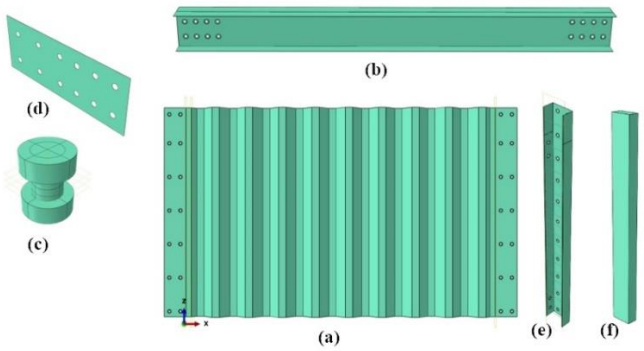

(a) corrugated plate;(b) beam; (c) bolt; (d) connection plate;
(e) steel column;(f) concrete;

Fig 15 The unit figure of the finite element model

3.2. FEA validation

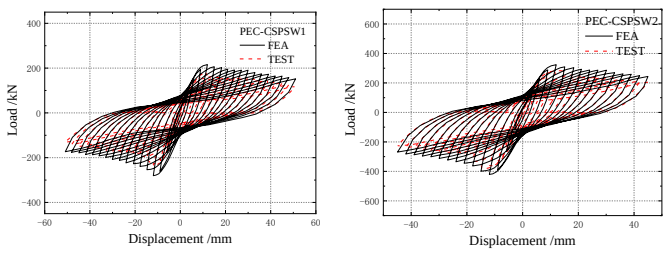

Fig. 16 Hysteretic curves of test and FEA results

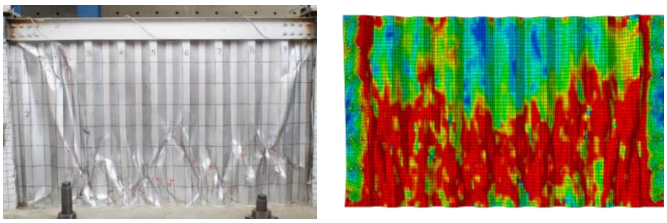

Fig. 17 Mises stress contrast nephogram of test and FEA results.

The study compares the experiment results of hysteretic curves and the FE model ,and it can be discovered that the specimen's initial stiffness was well predicted by the FEA method in Fig. 16. The two curves almost coincided when the displacement was small and also coincided well in the elastic-plastic stage. It was found that the specimen's stiffness, bearing capacity and hysteretic loop area calculated by the FEA method were slightly greater than the experimental results.This is because the influence of adverse conditions such as repeated bending and tearing of SPSWs and weld cracking was not considered in the finite element simulation. The hysteretic curve of the finite element model in the figure showed no obvious descending section after arriving at the peak load. In addition, the steel material constitutive model in the FEA model did not consider the material stiffness degradation and fracture caused by cyclic loading under the high stress state, and the hysteresis curve calculated by the finite element model was relatively full and the degree of "pinch" was relatively light. On the other hand, the residual stress accumulated during specimen processing and the inevitable existence of loading eccentricity in the loading process will reduce the test bearing capacity. But generally the finite element model well simulates the feature of SPSWs under cyclic loading, showing that the analysis method adopted in this paper was reliable.

Fig.17 demonstrates the Von Mises stress contrast nephogram for the experimental and FEA model at a lateral drift of 3.75%. It reveals that the yield distribution of plate in the test is primarily similar to the simulation results in the FEA, and the shear yield of steel plate is mostly concentrated in the lower region of steel plate and develops toward the ends of two columns. The yield area of the steel plate in test is minor than that of the finite element model, especially in the area near the edge column. This is because the edge frame has a better restraining effect on the corrugated steel plate in the FE simulation.

3.3. Parametric investigation

Based on the verified FEA method, to further research the impact of plate height-thickness ratio, wavelength, wave amplitude (Fig.18), and concrete strength grade on the lateral bearing capacity of PEC-CSPSWs, 26 finite element models were established in this paper. See Table 5 for the parameters of the models.

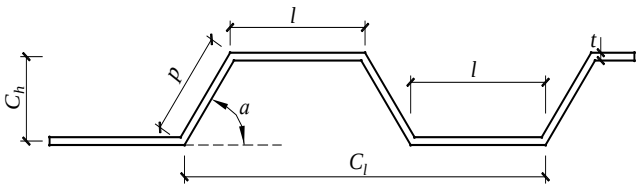

Fig. 18 Diagram of trapezoidal corrugated steel plate

Fig. 19 displays the skeleton curves of each group of specimens under cyclic loading. We can spot from the figure that the initial lateral stiffness of PEC-CSPSWs was roughly the same, and the skeleton curve showed an obvious S-shape, showing good lateral resistance. The structural bearing capacity increased slightly along with the growth of thickness and the corrugated steel plate wave amplitude. In addition, the initial stiffness of PEC-CSPSWs decreased gradually as the corrugated steel plate wavelength accumulated.

Fig. 20 displays the degradation curve of the secant stiffness of each specimen with loading displacement. Each model's stiffness degradation was obvious, and the change law was similar: the equivalent stiffness decreased gradually as the displacement increased, and the initial decline speed was faster. When the displacement was greater than 20mm, the decline speed slowed down and gradually became stable. After loading, the equivalent stiffness value of each specimen was the lowest, all about 5 kN/mm.

In Table 6, the energy dissipation coefficients of each model are listed. As the steel plate's thickness increased, the shape of the hysteresis loop became full, the energy dissipation coefficient increased, and the energy dissipation capacity

gradually increased. Models with different wavelengths and amplitudes had excellent energy dissipation performance, and their energy dissipation coefficients were similar, all around 4.0.

Fig. 21shows the Von-Mises stress distribution at the ultimate displacement of corrugated wallboard subjected to cyclic loading with different design parameters. Referring to Fig. 21(a)~(c), under cyclic loading, the value of the initial stiffness of the thin steel plate was smaller than that of the thick steel plate, the steel plate buckling occurred faster, and the distribution of "X" tensile bands was more. From Fig. 21(d)~(f), when the wavelength increased, the quantity of tensile bands decreased, and the stress on the steel plate surface increased. The reason for this is that with the growth of the steel plate wavelength, the number of ripples decreased, and the effective area for the steel plate to participate in the shear yield became smaller.This led to the steel plate early buckling and the bearing capacity decline. Fig. 21(g)~(i) shows that the number of tensile bands in the plate with a small wave amplitude was less, while the distribution of tensile bands in the plate with a large wave amplitude was more, basically covering the whole plate surface. This is because the out-of -plane stiffness of the steel plate which has small wave amplitude was small. Under reciprocating loading, a single "X" type tensile band was easier to form and the coverage area was increasingly large.

Table 5
Geometry parameters of PEC-CSPSW

Item	t/mm	λ	C_l /mm	C_h /mm	Column section/mm	C_g
P-CS1	1	1120	240	50	120×60×5	C30
P-CS2	1.5	747	240	50	120×60×5	C30
P-CS3	2	560	240	50	120×60×5	C30
P-CS4	2.5	448	240	50	120×60×5	C30
P-CS5	3	373	240	50	120×60×5	C30
P-CS6	3.5	320	240	50	120×60×5	C30
P-CS7	2	560	200	50	120×60×5	C30
P-CS8	2	560	220	50	120×60×5	C30
P-CS9	2	560	240	50	120×60×5	C30
P-CS10	2	560	260	50	120×60×5	C30
P-CS11	2	560	280	50	120×60×5	C30
P-CS12	2	560	300	50	120×60×5	C30
P-CS13	2	560	240	50	120×60×5	C30
P-CS14	2	560	240	60	120×60×5	C30
P-CS15	2	560	240	70	120×60×5	C30
P-CS16	2	560	240	80	120×60×5	C30
P-CS17	2	560	240	90	120×60×5	C30
P-CS18	2	560	240	100	120×60×5	C30
P-CS19	2	560	240	50	120×60×5	no-concrete
P-CS20	2	560	240	50	120×60×5	C25
P-CS21	2	560	240	50	120×60×5	C30
P-CS22	2	560	240	50	120×60×5	C40
P-CS23	2	560	240	50	120×60×5	C50
P-CS24	2	560	240	50	120×60×5	C60
P-CS25	2	560	240	50	120×60×5	C70
P-CS26	2	560	240	50	120×60×5	C80

Table 6
Energy consumption coefficient of models

Item	E	Item	E
P-CS1	3.54	P-CS14	3.99
P-CS2	3.20	P-CS15	4.07
P-CS3	3.96	P-CS16	4.02
P-CS4	4.10	P-CS17	4.03
P-CS5	4.12	P-CS18	3.85
P-CS6	4.93	P-CS19	3.84
P-CS7	4.07	P-CS20	3.99
P-CS8	3.96	P-CS21	3.90
P-CS9	3.96	P-CS22	3.77
P-CS10	3.89	P-CS23	3.73
P-CS11	3.85	P-CS24	3.63
P-CS12	3.57	P-CS25	3.64
P-CS13	3.96	P-CS26	3.65

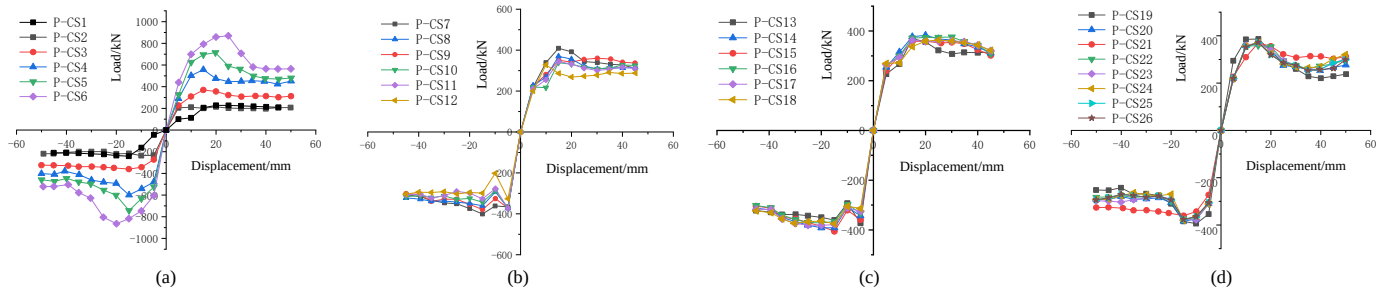

(a) (b) (c) (d)

Fig. 19 Skeleton curves of the model

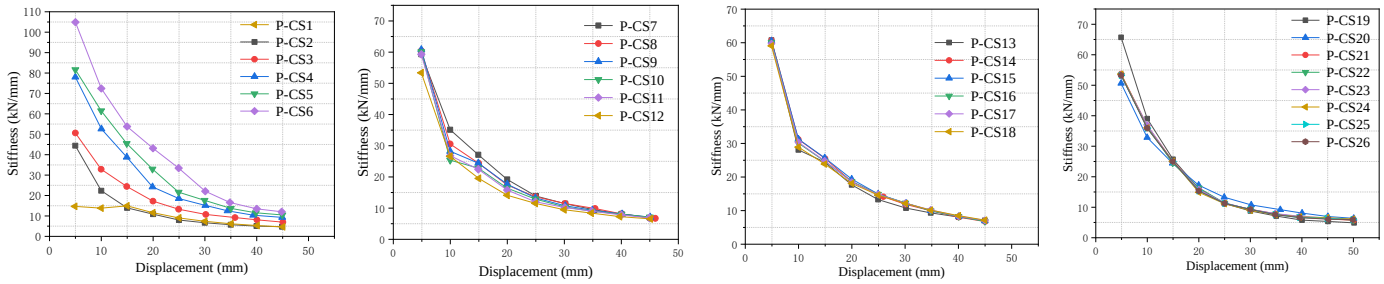

(a) (b) (c) (d)

Fig. 20 Stiffness degradation curves of models

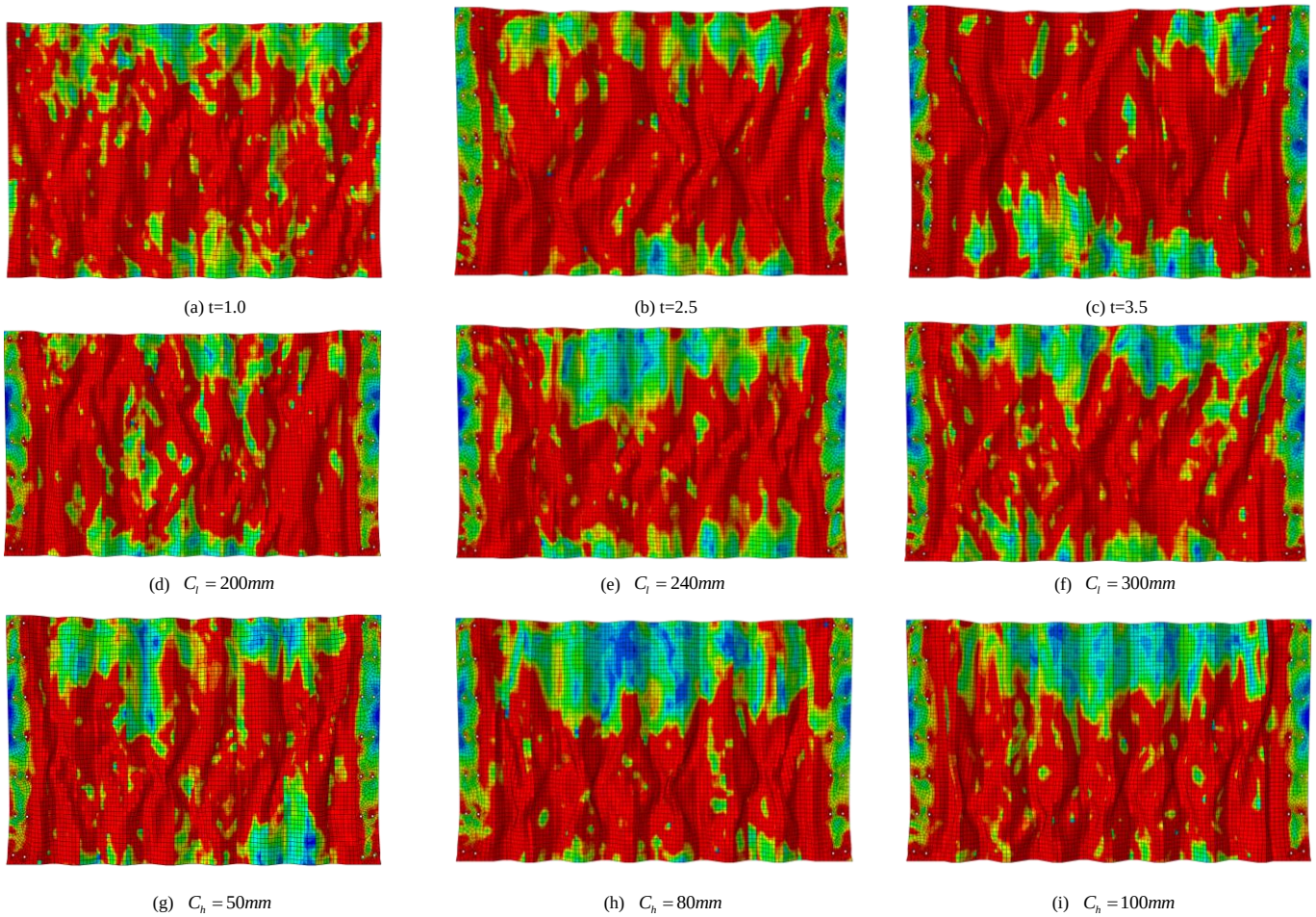

(a) t=1.0 (b) t=2.5 (c) t=3.5

(d) $C_l = 200mm$ (e) $C_l = 240mm$ (f) $C_l = 300mm$

(g) $C_h = 50mm$ (h) $C_h = 80mm$ (i) $C_h = 100mm$

Fig. 21 Von Mises stress distribution of the corrugated plate under cyclic loading

4. Conclusions

A new CSPSWs type was suggested in this paper, and two different types of specimens were designed. The seismic performance of the specimens was studied by a low-cycle reciprocating loading test, and reached the following conclusions:

(1) The trapezoidal CSPSWs with PEC columns connected by bolts had a high bearing capacity and lateral stiffness and had good hysteretic performance under cyclic loading. PEC column avoided the bending, torsion and buckling failure modes of pure steel column outside the plane, and formed the failure mode of “strong frame, weak wallboard, strong column and weak beam” in the plane. This structure could better meet the requirements of a double lateral force resistance design requirements; that is, the efficiency loss of the plate was before that of the boundary frame.

(2) The CSPSWs with PEC columns achieved post-yield buckling, and the

tension band formed after buckling continued to bear the load. The damaged parts of the specimens were concentrated in the middle of the wallboard, and the corner connection was not damaged. This indicates that the design of the fabricated connection structure proposed in this paper is reasonable and reliable.

(3) With the height-thickness ratio decrease of the corrugated steel plate, the ultimate bearing capacity of PEC-CSPSW increased and the initial lateral stiffness increased. The increase of wavelength and wave amplitude of the corrugated steel plate had little influence on the ultimate bearing capacity and initial lateral stiffness of PEC-CSPSW. In addition, the concrete addition enhanced the anchoring effect of side columns on the shear field of embedded steel plates, gave full play to the post-buckling strength of embedded steel plates, and obviously improved the bearing capacity and initial stiffness of the structure.

References

[1] Berman JW. and Bruneau M., "Experimental investigation of light-gauge steel plate shear walls", Journal of Structural Engineering, 131(2),259-267, 2005.

[2] Botros RBG. "Nonlinear finite element analysis of corrugated steel plate shear walls", Calgary，Alberta: University of Calgary, 62-109, 2006.

[3] Lan Y.J., "Research of resist lateral force structure-steel corrugated plate shear wall", MS Thesis, Xi'an University of Architecture and Technology,Xian,China, 2006. (in Chinese)

[4] Lu Y. and Li G.Q., "Slim buckling-restrained steel plate shear wall and simplified model", Advanced Steel Construction, 8(3),282-294, 2012.

[5] Stajadinovic B. and Tipping S., "Structural testing of corrugated sheet steel shear walls", Proceedings of the 9th International Specialty Conference on Cold-Formed Steel Structures St Louis, Missouri, USA: American Iron and Steel Institute, 425-439, 2008.

[6] L.A. Fülöp. and I. Hakola., "Design method for light-gauge steel shear walls sheathed with flat steel plates", Advanced Steel Construction, 3(3),628-651, 2007.

[7] Johnson RP., Cafolla J. and Bernard C., "Corrugated webs in plate girders for bridges", Structures and Buildings, 122(2),161, 1997.

[8] Liu S. M., Ding H. S., Taerwe L. and Corte W. D., "Modifications to the global and interactive shear buckling analysis methods of trapezoidal corrugated steel webs for bridges", Advanced Steel Construction, 15(4),349-363, 2019.

[9] Zhao Q.H, Sun J.H, Li Y.N. and Li Z.X., "Cyclic analyses of corrugated steel plate shear wall", The Structural Design of Tall and Special Buildings, 26(16), e1351, 2017.

[10] Dou C., Jiang Z.Q., Pi Y.L. and Guo Y L., "Elastic shear buckling of sinusoidally corrugated steel plate shear wall". Engineering Structures, 121,136-146, 2016.

[11] Dou C., Pi Y.L. and Gao. W., "Shear resistance and post-buckling behavior of corrugated panels in steel plate shear walls", Thin Walled Structures, 131, 816-826, 2018.

[12] Cao Q. and Huang J.Y., "Experimental study and numerical simulation of corrugated steel plate shear walls subjected to cyclic loads", Thin Walled Structures, 127,306-317, 2018.

[13] Yu J.G., Feng X.T.,Li B.,Hao J P. and Ge M.L., "Performance of steel plate shear walls with axially loaded vertical boundary elements", Thin-Walled Structure, 125(14), 152-163, 2018.

[14] Yu J.G. and Hao J.P., "Behaviour of semi-rigid steel frames with steel plate shear walls", Advanced Steel Construction, 12(2), 154-173, 2016.

[15] Chen Z.Y., Bian G.Q. and Huang Y., "Review on web buckling and hysteretic behavior of shear panel dampers", Advanced Steel Construction, 9(3),205-217, 2013.

[16] Piquer A. and Hernández-Figueirido D., "Protected steel columns vs partially encased columns: Fire resistance and economic considerations", Journal of Constructional Steel Research, 124,47-56, 2016.

[17] Song Y.C., Wang R.P. and Li J., "Local and post-local buckling behavior of welded steel shapes in partially encased composite columns", Thin-Walled Structures, 108(9), 93-108, 2016.

[18] Zhao G.T., Zhang Y.M., Cao F.B. and Zhou Y.H., "Experimental study on seismic performance of welded H-section steel partially encased columns with high strength concrete", Journal of Building Structures, 40(04), 116-122, 2019. (in Chinese)

[19] Chicoine T, Tremblay R, Massicotte B, Ricles J.M. and Lu L.W., "Behaviour and strength of partially encased composite columns with built up shapes", Journal of Structural Engineering, 128(3), 279-288, 2002.

[20] Feng J., Jin J., Xia J. and Fang Y.Z., "Experimental study on seismic performance of pec composite column-steel beam frame with welded t-stub strengthened connections", Advanced Steel Construction, 17(3), 264-272, 2021.

[21] Yin Z.Z., Li J.M. and Zhao S.P., "Experimental study of seismic behavior on steel plate shear wall with PEC columns", China Civil Engineering Journal, 51(S1), 139-144, 2018. (in Chinese)

[22] Yu J.G., Yu H.S., Feng X.T., Dang C.,Hou T.F. and Shen J., "Behaviour of steel plate shear walls with different types of partially-encased H-section columns", Journal of Constructional Steel Research, 170, 106123, 2020.

[23] Yin Z.Z., Zhang H. and Yang W.W., "Study on Seismic Performance and Damage Analysis of Steel Plate Shear Wall with Partially Encased Composite (PEC) Columns", Applied Sciences, 9(5), 907, 2019.

[24] JGJ/T 101-2015. Specification for Seismic Test of Buildings., China Architecture Industry Press, Beijing, China,2015.

[25] Han L.H. "Concrete-filled steel tube-theory and practice", 2nd ed. Beijing: Science Press, 2007:106. (in Chinese)

Acknowledgments

The financial supports from the National Natural Science Fund of China under grant No. 51968044 and research Project (JK2021-22，JK2022-06) of Gansu provincial department of housing and urban and rural construction are gratefully acknowledged.